Modeling and Simulation of a CMOS-MEMS Infrared Thermopile for Biomedical Applications

A. Martínez-Torteya, G. Dieck-Assad, S.O. Martínez-Chapa, S. Camacho-León
Electrical and Computer Engineering Department
Tecnológico de Monterrey, Campus Monterrey

Abstract

Thermopiles have several advantages for working as infrared radiation sensors and have already been used for applications in the biomedical diagnostics area. When designing thermopiles, it is of great importance to acknowledge the changes in the output voltage that the varying of each design variable may generate. This paper develops an accurate mathematical model for a thermopile with a bridge or cantilever structure, having a maximum error of 4.69% when compared with a finite element analysis simulation. The proposed model will be used to perform a parameter specific design optimization of a CMOS-MEMS infrared thermopile for biomedical applications.

Keywords: Infrared thermopile, CMOS-MEMS, bridge-MEMS, cantilever-MEMS

Resumen

Las termopilas tienen diversas ventajas para trabajar como sensores de radiación infrarroja y ya han sido usadas para distintas aplicaciones en el área de diagnóstico biomédico. Cuando se diseñan termopilas, es de gran importancia el identificar los cambios en el voltaje de salida que la variación de las variables de diseño pueden generar. En este artículo se desarrolla un modelo matemático preciso para una termopila con estructura en forma de puente y de viga, obteniendo un error máximo de 4.69% al comparar sus resultados con una simulación de análisis de elemento finito. El modelo propuesto será usado para optimizar el diseño de una termopila infrarroja CMOM-MEMS para aplicaciones biomédicas.

Palabras clave: Termopila infrarroja, CMOM-MEMS, puente-MEMS, viga-MEMS

Introduction

Non-invasive glucose monitor devices have been proposed using instantaneous differential near infrared (IR) spectrophotometry [1]. This scheme requires the integration of a micro CMOS-MEMS infrared thermopile sensor. An adequate modeling and simulation of the thermopile sensor is necessary to predict the proper behavior of the device and to develop the required signal processing hardware/software. The thermopile model is based fundamentally on the Seebeck effect, which describes the thermoelectric phenomena when self-generating temperature transducers convert temperature differences directly into electrical voltages without an external power supply. One of the first applications of thermoelectricity was the IR detector, and modern microsensors based on this effect have been fabricated using silicon micromachining, thin film technology and photolithography patterning [2].

When an electrically conducting material is placed with both ends at different temperatures, a voltage known as the net Seebeck electromotive force (emf) is generated between the ends of the material. The ratio of the net change of Seebeck emf that results from a temperature difference in a single material is called the absolute Seebeck coefficient α, and is described as:

$$\alpha = \frac{\Delta V}{\Delta T} \tag{1}$$

where ΔV is the change in the net Seebeck emf and ΔT is the temperature difference between ends of the material [3].

When two dissimilar thermoelectric materials are joined at both ends and one end is heated, there is a continuous current which flows in the circuit. If this circuit is broken, the open circuit voltage is a function of the junction temperature and the Seebeck effect of the two materials [4]. This specific configuration is known as the basic thermocouple and it is shown in Figure 1. The output voltage V_{AB} of the thermocouple is obtained through Kirchhoff's Law:

$$V_{AB} = V_A - V_B = (T_H - T_C)\alpha_A - (T_H - T_C)\alpha_B = \Delta T \alpha_{AB} \tag{2}$$

where ΔT is the temperature difference between the hot and cold junctions and α_{AB} is the difference between the absolute Seebeck coefficients of the materials, also known as the relative Seebeck coefficient of the material pair.
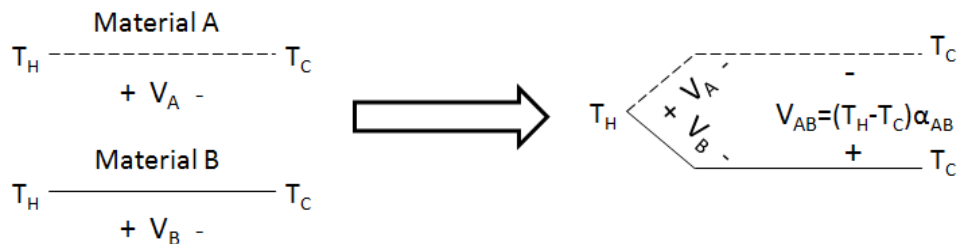

Figure 1. Basic thermocouple

A thermopile, as the one shown in Figure 2, is an array of thermocouples connected thermally in parallel, but electrically in series. Connecting z thermocouples in such a way increments the output voltage z times. Thus, the output voltage obtained with a thermopile, taking Equation (2) into account, is described by:

$$V_{thermopile} = zV_{thermocouple} = z\Delta T\alpha_{AB} \tag{3}$$
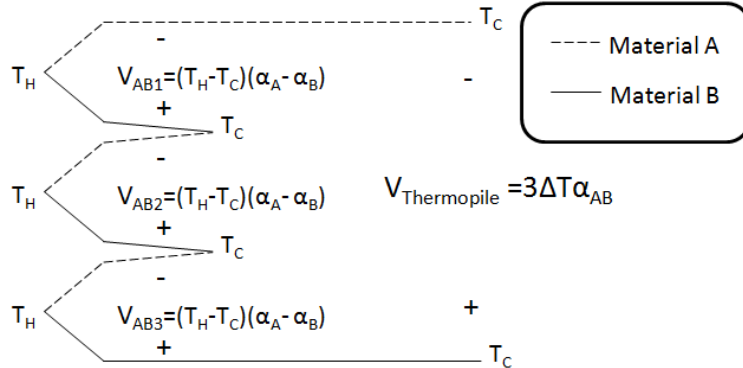
Figure 2. Basic structure of a thermopile with z=3

When fabricating thermopiles in a microscale, usually a thin membrane is connected to a silicon bulk working as a heat sink. Incident IR radiation rises the temperature of the membrane creating a temperature difference between hot (on the membrane) and cold (on the bulk) junctions. This temperature difference, as stated in Equation (3), generates a voltage proportional to the temperature difference itself, to the number of thermocouples, and to the relative Seebeck coefficient of the material pair.

This implies that there are three main ways in which the thermopile could be modified to achieve a larger voltage, and thus a better sensitivity: incrementing the number of thermocouples, creating a larger difference between Seebeck coefficients by choosing different materials and incrementing the temperature difference by creating a high thermal insulation of the hot junctions. This paper develops an accurate mathematical model for a thermopile with a cantilever structure, which takes into account these three characteristics, and also the geometric parameters of the thermocouples.

Model Development

To better understand the behavior of a sensor and to optimize its performance, a mathematical model is needed. Some efforts have been reported to model and simulate an overall integrated thermopile sensor system [5, 6]. However, a mathematical model for the sensitivity of thermopile infrared detectors on CMOS silicon oxide cantilever beams, isolated by a post-processing anisotropic etching, was obtained by [7], which was the basis for the proposed analytical model developed here. In this structure, shown in Figure 3, while the hot contacts are located at the tip of the membrane, the cold contacts are located at the bulk, working as a heat sink.
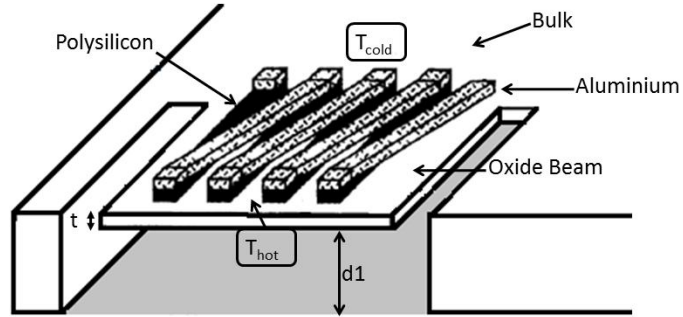
Figure 3. Thermopile infrared detector on CMOS silicon oxide cantilever beam isolated by post-processing anisotropic etching [7]

For all simulation and performance purposes, the materials that were considered for the thermocouples were n-poly-Si and p-poly-Si. Since Si is transparent to IR radiation above 1 μm [8] and the intended application of this device uses an IR source with a larger wavelength, the hot junctions need to be coated, or in contact with a black absorber film, whose dimensions define the sensitive area of the sensor. This film will absorb the IR radiation and increase its temperature, increasing also the temperature of the materials in the hot junction.
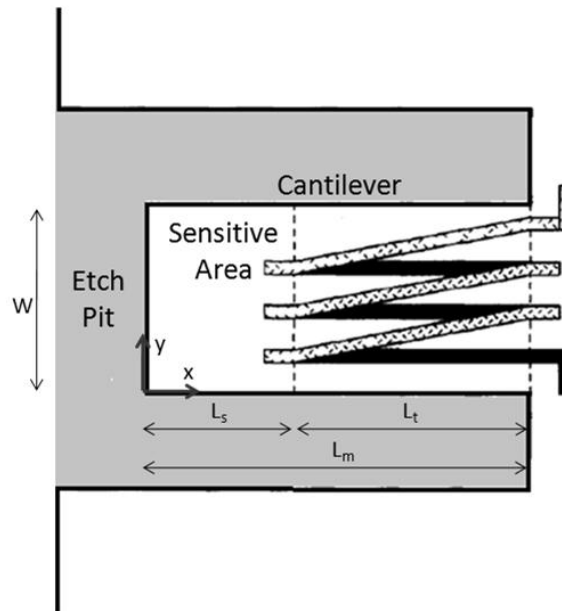
Figure 4. Top view of cantilever thermopile [7]

To obtain the analytical model, first the geometry related variables were defined as shown in Figure 4. In order to calculate the sensitivity, the temperature distribution along the cantilever in the x-direction had to be known. Neglecting the boundary disturbances in the y-direction, the Joule heating effect, assuming a uniform thermal conductivity, a uniform temperature across the thin cantilever, and assuming all terms remain constant for $L_s \leq x \leq L_m$, the temperature distribution along the cantilever in the x direction was defined as:

$$\frac{d^2(T(x) - T_e)}{dx^2} + \frac{A\sigma(\varepsilon_t + \varepsilon_b)(T^4(x) - T_e^{\,4})}{cV} + \frac{\gamma A(T(x) - T_e)}{cV} = 0 \tag{4}$$

where the three terms represent the heat loss due to conductivity, to radiation, and to convection, respectively. Also, the radiation term only takes into account the radiation heat loss on the upper and lower faces of the membrane. Since the area of the side faces is much smaller than the area of the upper and lower faces, the heat loss on these surfaces is negligible.

In Equation (4), x is the variable distance along the membrane, T_e is the environmental temperature, A is the area of the membrane in the x-y plane, σ is the Stefan-Boltzmann constant, ε_t is the emissivity of the upper face of the membrane, ε_b is the emissivity of the lower face of the membrane, γ is the convective heat transfer coefficient of the gas atmosphere, c is the thermal conductivity of the cantilever material (also called λ by some authors) and V is the volume of the membrane. The heat transfer coefficient was defined as:

$$\gamma = c_g \left(\frac{1}{d_1} + \frac{1}{d_2} \right) \tag{5}$$

where c_g is the thermal conductivity of the gas atmosphere, d_1 is the distance between the membrane and the bottom of the etch pit, as shown in Figure 3. Thermopile infrared detector on CMOS silicon oxide cantilever beam isolated by post-processing anisotropic etching [7], and d_2 is the distance between the membrane and the package cap.

Inserting Equation (5) in Equation (4), and considering that:

$$V = WL_m t = At \tag{6}$$

where, W is the width of the membrane, L_m is the length of the beam and t is the thickness of the membrane, and also factorizing and expanding the radiation term of Equation (4) as:

$$\left(T^4(x) - T_e^{\,4}\right) = (T(x) - T_e)\left(T^3(x) + T^2(x)T_e + T(x)T^2{}_e + T_e^{\,3}\right) = 4T_e^{\,3}(T(x) - T_e) \tag{7}$$

and assuming that:

$$T(x) \approx T_e \tag{8}$$

we obtained:

$$\frac{d^2(T(x) - T_e)}{dx^2} + \left[\frac{4(\varepsilon_t + \varepsilon_b)\sigma T_e^{\,3} + c_g \left(\frac{1}{d_1} + \frac{1}{d_2} \right)}{ct} \right](T(x) - T_e) = 0 \tag{9}$$

To find a solution for Equation (9), it is first rewritten as:

$$\frac{d^2F(x)}{dx^2} = -k^2 F(x) \tag{10}$$

where:

$$k = \sqrt{\frac{4(\varepsilon_t + \varepsilon_b)\sigma T_e{}^3 + c_g\left(\frac{1}{d_1} + \frac{1}{d_2}\right)}{ct}} \tag{11}$$

and:

$$F(x) = T(x) - T_e \tag{12}$$

Solving Equation (10) yields:

$$(D^2 + k^2)F(x) = 0 \tag{13}$$

thus, the general solution is:

$$F(x) = C_1 e^{kx} + C_2 e^{-kx} = D_1\left(\frac{e^{kx} + e^{-kx}}{2}\right) + D_2\left(\frac{e^{kx} - e^{-kx}}{2}\right) \tag{14}$$

where:

$$C_1 = \frac{D_1 + D_2}{2} \tag{15}$$

$$C_2 = \frac{D_1 - D_2}{2} \tag{16}$$

and by applying Euler's identity and trigonometric identities, Equation (14) turned into:

$$F(x) = A \sinh\big(k(L_m - x)\big) \tag{17}$$

It can be demonstrated that Equation (17) is in fact a solution for Equation (10), considering that:

$$\frac{dF(x)}{dx} = -kA \cosh\big(k(L_m - x)\big) \tag{18}$$

thus,

$$\frac{d^2F(x)}{dx^2} = -k^2 A \sinh\big(k(L_m - x)\big) = -k^2 F(x) \tag{19}$$

Assuming temperature at L_m equals environmental temperature, and temperature at L_s, as defined by Figure 3, equals the temperature at the sensitive area, the boundary conditions were defined as:

$$[T(x) - T_e]_{x=L_m} = A \sinh\big(k(L_m - L_m)\big) = 0 \tag{20}$$

and

$$[T(x) - T_e]_{x=L_s} = A \sinh\big(k(L_m - L_s)\big) = T_s - T_e \tag{21}$$

where T_s is the temperature at the sensitive area.

Solving for A in Equation (21) yielded:

$$A = \frac{T_s - T_e}{sinh\big(k(L_m - L_s)\big)}$$ (22)

and by inserting Equation (22) in Equation (17), the temperature distribution was obtained:

$$T(x) - T_e = \frac{sinh\big(k(L_m - x)\big)}{sinh\big(k(L_m - L_s)\big)}(T_s - T_e)$$ (23)

The temperature increase was then calculated using the heat-balance condition:

$$-\left[W\lambda t \frac{dT(x)}{dx}\right]_{x=L_s} = \left\{\varepsilon_t E - \left[4(\varepsilon_t + \varepsilon_b)\sigma T_e^{\ 3} + \gamma\right](T_s - T_e)\right\}WL_s$$ (24)

where E is the irradiance given in W/m². To solve such equation for $(T_s - T_e)$, the f the first derivative of $T(x)$ was obtained:

$$\left.\frac{dT(x)}{dx}\right|_{x=L_s} = -k\frac{cosh\big(k(L_m - L_s)\big)}{sinh\big(k(L_m - L_s)\big)}(T_s - T_e) = -k\,coth\big(k(L_m - L_s)\big)\,(T_s - T_e)$$ (25)

and by inserting Equation (25) in Equation (24) we obtained:

$$W\lambda tk(T_s - T_e)\,coth\big(k(L_m - L_s)\big) = \left\{\varepsilon_t E - \left[4(\varepsilon_t + \varepsilon_b)\sigma T_e^{\ 3} + \gamma\right](T_s - T_e)\right\}WL_s$$ (26)

The temperature increase equation was found by solving Equation (26) for $(T_s - T_e)$:

$$(T_s - T_e) = \frac{\varepsilon_t E}{\left[4(\varepsilon_t + \varepsilon_b)\sigma T_e^{\ 3} + \gamma\right] + \frac{kct}{L_s}\,coth\big(k(L_m - L_s)\big)}$$ (27)

The sensitivity for a thermal detector is defined as the ratio of the signal voltage U to the incident radiation power P. The signal voltage was defined in Equation (3), and the incident radiation power is given by:

$$P = EWL_s$$ (28)

thus, the sensitivity of the system is:

$$S = \frac{U}{P} = \frac{\varepsilon_t z\alpha}{\left[4(\varepsilon_t + \varepsilon_b)\sigma T_e^{\ 3} + \gamma\right]WL_s + Wkct\,coth\big(k(L_m - L_s)\big)}$$ (29)

Optimization of the geometry of the thermopile is critical to achieve a good performance of this device. Because of this, it is of interest to study how the width, length, number and thermal properties of the thermocouples affect the behavior of the sensor. But, Equation (24) does not take into account some of these parameters. Thus, modifications to the model had to be made in order to insert these variables and to analyze them in terms of the performance of the thermopile.

Regarding the analytical model, thermopiles can be thought of as part of the membrane, constituting a bi-layer membrane with different characteristics than the one modeled previously. This means that modifying a parameter such as the thickness of the membrane would translate into a change of temperature proportional to the one achieved by varying the thickness of the thermocouples. To prove this hypothesis, generic thermopiles, as the one shown in Figure 5, were designed using the finite element analysis environment, COMSOL. The basic structure consists of a Si_3N_4 cantilever membrane on a Si bulk, with two n-poly-Si/p-poly-Si thermocouples denoted by the blue and red colors respectively, and a sensitive area denoted by the color aqua. The specific values of the geometry parameters used for such simulation are shown in Table I.

Table I. Values of the geometry parameters used in the COMSOL design shown in Figure 5

Parameter	Value [μm]
$W_{membrane}$	36
$W_{thermocouple}$	4
$L_{membrane}$	900
$L_{thermocouple}$	650
$L_{sensitive\ area}$	250
$t_{membrane}$	.5 to 1
$t_{thermocouple}$	.5 to 1
d_1	350
d_2	∞
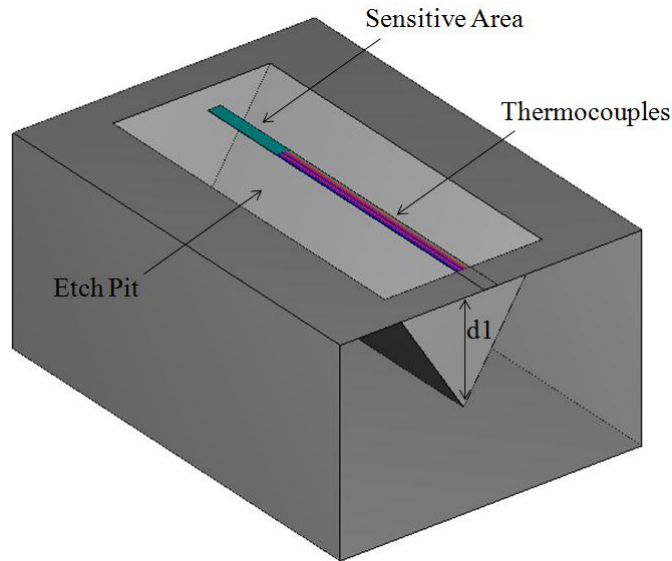
Figure 5. Cantilever thermopile designed in COMSOL. Anterior face suppressed for visualization purposes

Twelve thermopiles were designed, six with a fixed membrane thickness of 800 nm, but with a thermocouple thickness varying from 500 to 1000 nm with 100 nm steps. The other six thermocouples had a fixed thermocouple thickness of 500 nm, but with a membrane thickness varying from 500 to 1000

nm with 100 nm steps. This design is illustrated in Figure 6, where the variation in the thicknesses of the thermocouples and the membrane are shown. The parameter d_2 was assumed as infinite since the package cap was not designed.


(a)

(c)

(b)

(d)
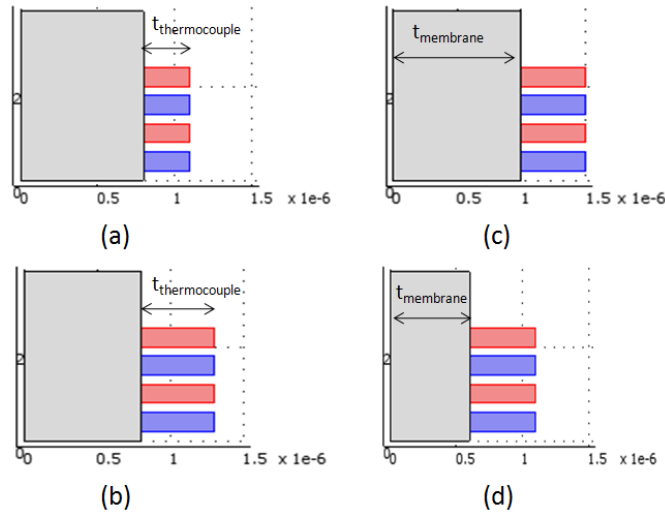
Figure 6. Thermocouples designed in COMSOL with (a) $t_{thermocouple}$ = 0.3 µm, $t_{membrane}$ = 0.8 µm, (b) $t_{thermocouple}$ = 0.5 µm, $t_{membrane}$ = 0.8 µm, (c) $t_{thermocouple}$ = 0.5 µm, $t_{membrane}$ = 1 µm, (d) $t_{thermocouple}$ = 0.5 µm, $t_{membrane}$ = 0.6 µm

A curve for the temperature at the sensitive area, as the one shown in Figure 7, was obtained for each thermopile designed. Using MATLAB, the maximum temperatures detected were normalized and plotted either as a function of the thickness of the thermocouples or of the membrane. Two similar curves were expected for the thermocouples to accurately be considered as part of the membrane in the analytical model.
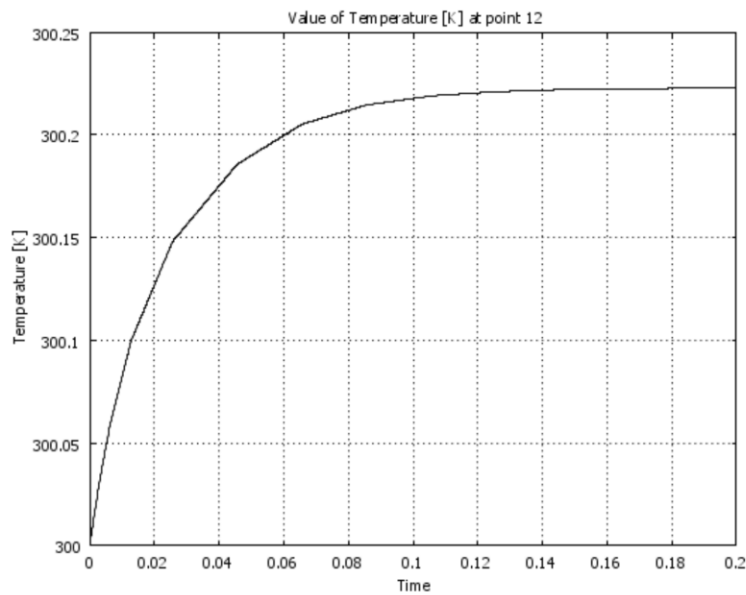
Figure 7. Temperature at the sensitive area of the thermopile shown in Figure 5 vs. time

The results obtained are shown in Figure 8, it can be seen that both parameters affect the temperature difference between the hot and cold junctions in the same manner, confirming the validity of the proposed hypothesis. The use of a normalized temperature instead of the obtained temperature itself is due to the fact that increasing or decreasing the thickness of the membrane by a specific value, will not generate the same change in the temperature as if the thickness of the thermocouples were increased or decreased by the same value, but it will be a proportional change.
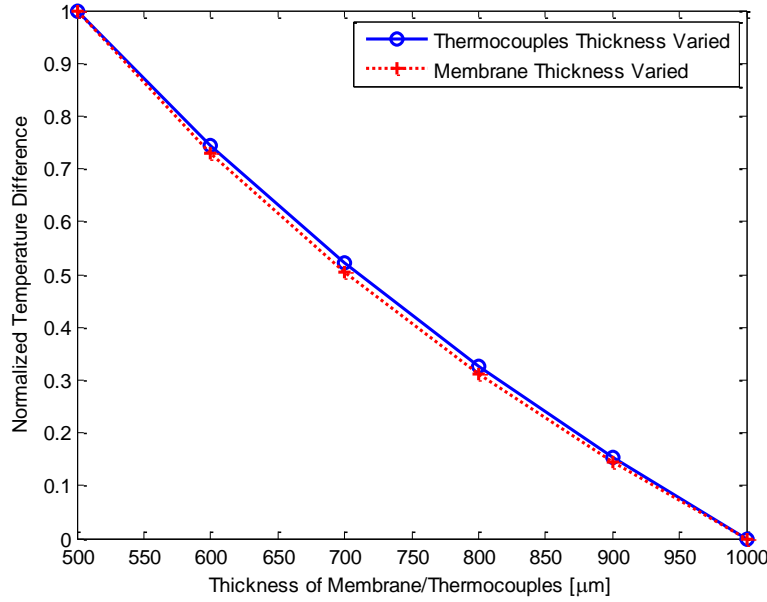
Figure 8. Relationship between the thickness of the thermocouples and the thickness of the membrane

To insert the parameters of the thermocouple in the analytical model, considering it as a component of the membrane, a few changes had to be made. Since the thermocouples, as a whole, have a non-rectangular geometry and are not as long as the beam, Equation (6) needed an additional term:

$$V = W_m L_m t_m + 2z W_t L_t t_t = V_m + V_t \qquad (30)$$

where W_m is the width of the membrane (previously called W), L_m is the length of the membrane, t_m is the thickness of the membrane (previously called t), W_t is the thickness of the thermocouples, L_t is the length of the thermocouples, t_t is the thickness of the thermocouples , V_m is the volume of the membrane as given by Equation (6), and V_t is the volume contribution of the thermocouples.

Because of this, the simplification:

$$\frac{cV}{A} = ct \qquad (31)$$

used in Equation (9) needed to be modified, and considering that the thermal conductivity of the bi-layered cantilever is defined as:

$$c = \frac{c_m t_m + c_t t_t}{t_m + t_t} \tag{32}$$

then, Equation (31) had to be changed to:

$$\frac{cV}{A} = \left(\frac{c_m t_m + c_t t_t}{t_m + t_t}\right)\left(\frac{V_m + V_t}{W_m L_m}\right) = \left(\frac{c_m t_m + c_t t_t}{t_m + t_t}\right)\left(t_m + \frac{V_t}{W_m L_m}\right) \tag{33}$$

thus, the new k parameter was defined as:

$$k = \sqrt{\frac{4(\varepsilon_t + \varepsilon_b)\sigma T_e^{\,3} + c_g\left(\frac{1}{d_1} + \frac{1}{d_2}\right)}{\left(\frac{c_m t_m + c_t t_t}{t_m + t_t}\right)\left(t_m + \frac{V_t}{W_m L_m}\right)}} \tag{34}$$

and consequently, the sensitivity for the proposed model became:

$$S = \frac{\varepsilon_t z \alpha}{\left[4(\varepsilon_t + \varepsilon_b)\sigma T_e^{\,3} + \gamma\right]W_m L_s + W_m k \left(\frac{c_m t_m + c_t t_t}{t_m + t_t}\right)\left(t_m + \frac{V_t}{W_m L_m}\right)\coth\big(k(L_m - L_s)\big)} \tag{35}$$

which shows that the sensitivity has a dependency on the geometry, the fabrication process, and the materials used.

Validation of the proposed model

The proposed analytical model was tested using MATLAB. The values of the parameters of the thermopile used for the simulations are shown in Table II. Those same parameters were used for designing a thermopile as the one shown in Figure 5 with COMSOL, so that the results of the analytical model obtained with MATLAB could be compared with the results of the structure analyzed using the finite element analysis.

Table II. Parameters of the thermopile used to validate the analytical model

Parameter	Value	Parameter	Value
ε_{top}	1	L_t	$650\,[\mu m]$
ε_{bottom}	0.5	L_s	$250\,[\mu m]$
P	$27\,[\mu W]$	L_m	$900\,[\mu m]$
T_e	$300\,[K]$	z	2
c_m	$20\,[W \cdot K^{-1} \cdot m^{-1}]$	α	$309.64\,[\mu V \cdot K^{-1}]$
c_t	$34\,[W \cdot K^{-1} \cdot m^{-1}]$	W_m	$36\,[\mu m]$
c_g	0	W_t	$4\,[\mu m]$
t_m	$0.5\,[\mu m]$	d_1	$350\,[\mu m]$
t_t	$0.5\,to\,1\,[\mu m]$	d_2	∞

In the simulation range, varying the thickness of the thermocouples from 500 to 1000 nm, a maximum error between the analytical and the finite element analysis for the temperature difference of 4.69% was obtained. Also, as shown in Figure 9, the behavior of both curves seems to be similar, which leads to the assumption that the error obtained between both methods is not due to the thickness of the thermocouples.
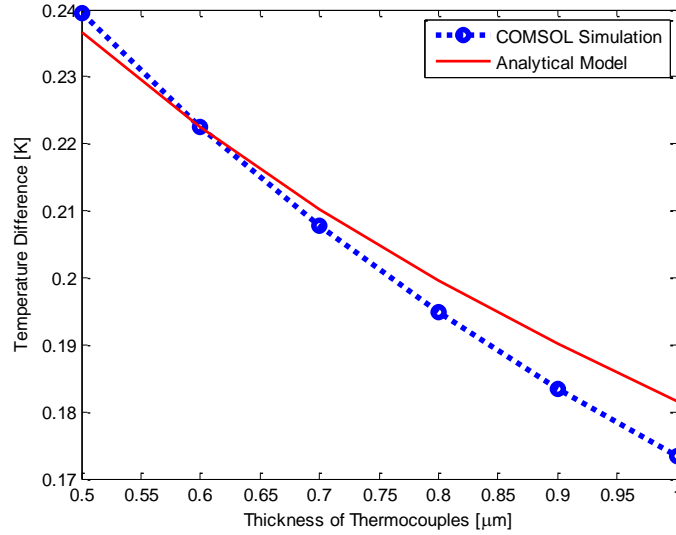
Figure 9. Temperature difference vs. thickness of the thermocouples for both the analytical and the finite element analysis

To better prove this hypothesis, the results were normalized in order to find the similarity in the behavior of both curves. The normalization consisted in subtracting the smallest value and dividing over the largest value minus the smallest value for each curve. With the normalized curves, as shown in Figure 10, a maximum error between curves of 1.73% was obtained, demonstrating that both curves respond in an almost identical way for a change in the thickness of the thermocouples. These results demonstrate that the proposed analytical model, can accurately determine the changes in the temperature difference that a change in the parameters of the thermocouple generates. Therefore, the output voltage and the sensitivity can also be accurately obtained.
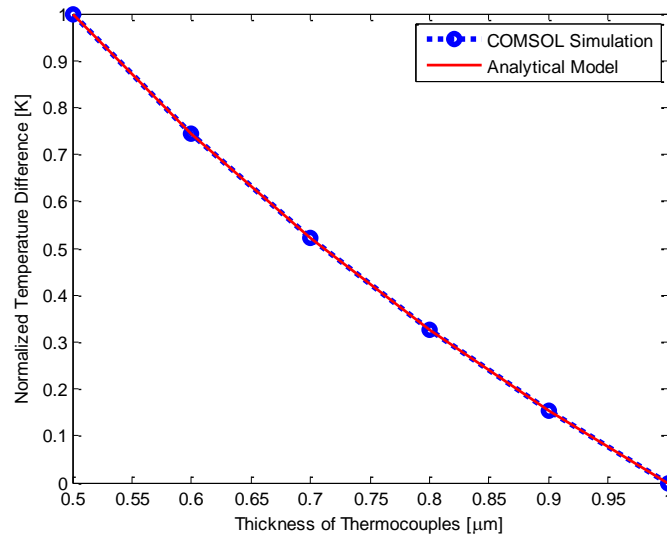
Figure 10. Normalized temperature difference vs. thickness of thermocouples for the analytical and the finite element analyses

Conclusions

A CMOS-MEMS thermopile model and simulation was presented in this paper. The proposed analytical model accurately describes the behavior of a thermopile based on a cantilever structure with a maximum error of 4.69%. Previous models did not include the geometry and material dependent parameters relative to the thermocouples. With the addition of such variables to the proposed model, a more precise analysis was done, which can be translated into an optimization of the geometry of the thermocouples. This model will be used to perform an optimization analysis having fabrication, material and design dependent parameters. This analysis is necessary to obtain the best possible design for the CMOS-MEMS based infrared thermopile sensor to be integrated in a non-invasive blood glucose monitor system.

Referencias

1. Yamakoshi, Y., et al. *A new non-invasive method for measuring blood glucose using instantaneous differential near infrared spectrophotometry*. IEEE.
2. Rowe, D.M., *General principles and basic considerations.* Thermoelectrics Handbook: Macro to Nano, 2006.
3. Measurement, A.C.E.-o.T. and A.C.E.-o.T.M.S.E.o. Thermocouples, *Manual on the use of thermocouples in temperature measurement*. 1981: ASTM International.
4. OMEGA, *The OMEGA® Complete Temperature Measurement Handbook and Encyclopedia*, OMEGA, Editor 2010.
5. Akin, T., et al., *An integrated thermopile structure with high responsivity using any standard CMOS process.* Sensors and Actuators A: Physical, 1998. **66**(1-3): p. 218-224.
6. Levin, A. *A numerical simulation tool for infrared thermopile detectors*. IEEE.
7. Elbel, T., R. Lenggenhager, and H. Baltes, *Model of thermoelectric radiation sensors made by CMOS and micromachining.* Sensors and Actuators A: Physical, 1992. **35**(2): p. 101-106.
8. Kong, S.H., et al., *Integrated silicon microspectrometers.* Instrumentation & Measurement Magazine, IEEE, 2001. **4**(3): p. 34-38.